JTTEE5 19:128–136
DOI: 10.1007/s11666-009-9447-6
1059-9630/$19.00 © ASM International

Effects of Some Light Alloying Elements on the Oxidation Behavior of Fe and Ni-Cr Based Alloys During Air Plasma Spraying

Zhensu Zeng, Seiji Kuroda, Jin Kawakita, Masayuki Komatsu, and Hidenori Era

(Submitted April 24, 2009; in revised form September 12, 2009)

The oxidation behavior of iron binary powders with addition of Si (1, 4 wt.%) and B (1, 3 wt.%) and that of a Ni-Cr based alloy powder with Si (4.3 wt.%), B (3.0 wt.%), and C (0.8 wt.%) additions during atmosphere plasma spray (APS) have been investigated. Analysis of the chemical composition and phases of oxides in the captured in-flight particles and deposited coatings was carried out. The results show that the addition of Si and B to iron effectively reduced the oxygen contents in the coatings, especially during the in-flight period at higher particles temperature. Ni-Cr based alloy powder with Si, B, and C additions reduced the oxidation of the base alloys significantly. Preferential oxidation and subsequent vaporization of Si, B, and C from the surface of the sprayed particles are believed to play a major role in controlling oxidation in the APS process.

Keywords air plasma spray, corrosion, evaporation, Fe-binary alloy, light alloying element, oxidation

1. Introduction

Thermal-sprayed metallic alloy coatings are used in a wide range of industries to improve the corrosion and wear resistance of machine components. The rapid cooling of sprayed powders from the melt in thermal spraying enables one to form coatings containing amorphous phases and nanocrystals. Fe-based alloys have attracted much attention in the spraying community because of their mechanical properties and corrosion resistance at relatively low material costs (Ref 1, 2). Ni-Cr alloys coatings are widely applied by thermal spraying to protect steel components in chemical plants, and boiler tubes in power plants and blades in turbine engines because of their good resistance against corrosion and high-temperature oxidation (Ref 3-6).

Among various application techniques, atmospheric plasma spraying (APS) is often used due to its high-deposition rate and relatively low-application costs. In the APS process, metallic alloy powders are heated to the melting state, and accelerated to impact the substrate. Oxidation of the particles occurs during the in-flight period (in-flight oxidation), which increases with increases in the spray distances (SDs). Another step of oxidation occurs at the moment of particle impact and solidification on-substrate surface (on-substrate oxidation), which is influenced by the particles size and the substrate temperature (Ref 7). The oxidation of Fe-based and Ni-Cr based alloys during APS process results in a significant amount of oxides remained in the coatings affecting the coating properties required in their service.

To protect iron and chromium from oxidation during thermal spray process, many efforts have been made, such as spraying alloy powders in the unmelted state with high-velocity air-fuel (HVAF) or cold spray (CS) system (Ref 8, 9). Even though oxidation can be essentially eliminated in these processes, the density of the coating tends to be insufficient and post-spray sealing is usually required. The oxidation problem is approached from the viewpoint of the feedstock material in this study.

It is generally known that carbon, silicon, and boron are elements with strong affinity for oxygen, which has been used in steel making process as de-oxidants by reacting with oxygen preferentially and consuming themselves by evaporation because they form volatile oxides at the operation temperature (Ref 10, 11). It is expected that addition of these elements in thermal spray powder alloys protects the main elements from oxidation during APS process.

The present article describes the effects of Si, B, and C on the oxidation of Fe-based and Ni-Cr based coatings during APS process. To better understand the effect of

This article is an invited paper selected from presentations at the 2009 International Thermal Spray Conference and has been expanded from the original presentation. It is simultaneously published in *Expanding Thermal Spray Performance to New Markets and Applications: Proceedings of the 2009 International Thermal Spray Conference*, Las Vegas, Nevada, USA, May 4-7, 2009, Basil R. Marple, Margaret M. Hyland, Yuk-Chiu Lau, Chang-Jiu Li, Rogerio S. Lima, and Ghislain Montavon, Ed., ASM International, Materials Park, OH, 2009.

Zhensu Zeng, Kurashiki Boring Kiko. Co., Ltd., 329-2 Ebana, Jitoukami, Kamogata-cho, Asakuchi-gun, Okayama 719-0233, Japan; **Seiji Kuroda, Jin Kawakita,** and **Masayuki Komatsu**, National Institute for Materials Science, 1-2-1, Sengen, Tsukuba, Ibaraki 305-0047, Japan; and **Hidenori Era**, Kyushu Institute of Technology, 1-1-1, Sensui, Kitakyushu, FukuokaJapan. Contact e-mail: zeng@kbknet.co.jp.

individual element on the complex oxidation process in APS, a simplified study for Fe-based alloys was performed by using binary alloys of Fe-Si and Fe-B powders, being compared with a commercially available stainless steel alloy. The knowledge about the oxidation behavior of these binary alloys can be useful in designing of more complex alloys with industrial importance.

The study of the effects of Si, B, and C on Ni-Cr based coatings was carried out using two commercial available powders of Ni20Cr and Ni-Cr based alloys containing Si, B, and C that is called as the self-fluxing alloys (SFA) in the field of thermal spray technology. The oxidation resistance and corrosion behavior of the Ni20Cr coating have been studied intensively by many researchers (Ref 3-5). However, the oxidation behaviors of the sprayed particles and coatings during thermal spraying have not been investigated separately. Since SFA alloys contain significant amount of Si, B, and C, it is of great interest to investigate their effects on the oxidation of the sprayed powders and the resultant coatings.

2. Experiment

In addition to commercially available powders of AISI 316L (Carpenter Powder Products GMBH), Ni20Cr and NiCrSiBC (Praxair, USA), iron, Fe- (1 and 4 wt.%) Si and Fe-(1 and 3 wt.%) B powders were gas atomized in our laboratory. The compositions of the Fe-based powders and Ni-based powders are shown in Table 1 and 2, respectively. The average particle diameters were approximately 37 μm. A DC plasma torch (SG-100, Praxair, USA) was used with the spray conditions shown in Table 3 for the Fe-based alloys and Ni-based alloys, respectively.

These Fe-based and Ni-Cr alloy powders were sprayed by using APS process with two power level, i.e., standard plasma power and low plasma power, respectively. The standard plasma power was chosen so that it can melt the Fe-based particles well for producing appropriate properties of the coatings. Spraying of Ni-Cr coatings was possible by the lower plasma power, because the SFA powder has a low-melting point (approximately 1050 °C), and even this plasma power is possible low for melting Ni20Cr powder (melting point approximately 1400 °C). To investigate the in-flight oxidation, samples sprayed at different SDs were analyzed even the standard SD is about 100 mm for the APS system. The oxidation of these alloy powders during spraying is compared by analyzing the captured in-flight particles as well as the sprayed coatings in terms of microstructure, chemical composition.

The sprayed particles were captured by quenching into liquid nitrogen at a SD of 100 and 200 mm (nozzle to liquid nitrogen level) as shown in Fig. 1. As it might be expected, the effective spraying distance for initial SD setting of 100 mm during the capturing experiments was approximately 80 mm because the liquid nitrogen level fell down by about 40 mm due to evaporation during the spraying period of 10 s, which was necessary to capture a sufficient amount of powder for analysis. The evaporation is negligible for the measuring of oxidation rate of the in-flight particles since same experiment was carried out by using quenching oil instead of liquid nitrogen. The oxygen

Table 1 Composition of Fe-based alloy feedstock powders

	Ni	Cr	B	Si	Fe	C	O
NiCrSiBC	Bal	15.3	3.02	4.31	3.4	0.8	0.032
Ni20Cr	Bal	21.4	···	0.41	···	0.011	0.026

Table 2 Composition of Ni-based alloy feedstock powders

	Fe	Ni	Cr	Si	B	C	O
SUS316L	Bal	11.1	19.6	0.40	···	0.025	0.023
Fe	Bal	···	···	0.14	···	0.007	0.014
Fe1Si	Bal	···	···	1.01	···	0.03	0.024
Fe4Si	Bal	···	···	4.03	···	0.02	0.011
Fe1B	Bal	···	···	···	0.98	0.05	0.010
Fe3B	Bal				3.01	0.034	0.012

Table 3 Spray parameters

	Fe-based alloy	Ni-based alloy
Argon flow rate, sl/min	50	50
Helium flow, sl/min	23.6	···
Voltage, V	33.0	27
Current, A	400	27
Powder feed argon flow rate, sl/min	5	5
Powder feed rate, g/min	30	30
Torch traverse velocity, mm/s	200	200

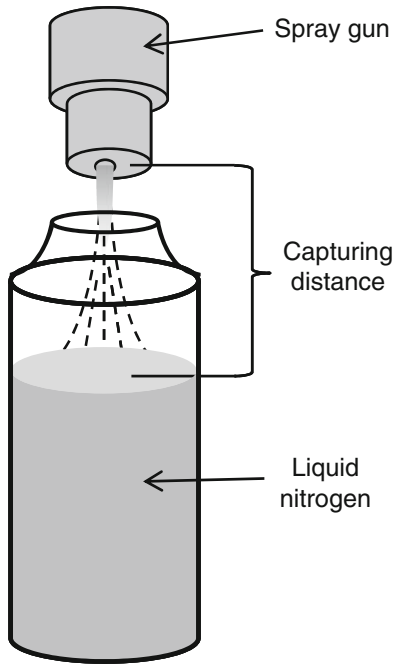

Fig. 1 Setup for capturing in-flight particles

content of the captured particles did not show any difference between the two quenching liquids. The container used was a double-walled insulating stainless steel bottle with 130 mm outer diameter and 250 mm height, having a circular opening of 50 mm diameter on the top. Before each experiment, the bottle was filled with liquid nitrogen up to the level of 4 mm from the top of the bottle.

The coatings were deposited at SDs of 50, 100, 150, and 200 mm for the Fe-based alloys and 100, 200 mm for the Ni-based alloys. The substrates were cooled by an air jet from the back during spray and the temperature were controlled to below 350 °C by a thermo-couple set in drilled hole in the substrates. The captured particles and sprayed coatings were examined by a scanning electron microscope (SEM) (JSM6500, JEOL, Japan) with an energy dispersible x-ray detector (EDX).

To assess the amount of oxygen and carbon, analysis was carried out by employing the infrared spectrometry with LECO TC-600 analyzer for oxygen and LECO CS444LS (LECO, USA) for carbon. Other elements were analyzed by an ICP optical emission spectrometer (ICPS2000 type, Shimadzu, Japan).

3. Results

3.1 Fe-Based Alloys

3.1.1 Cross Sections of Captured Particle. Figure 2 shows back-scattered electron (BSE) images of the cross sections of the captured AISI 316L, iron, Fe1Si, and Fe1B particles at SD of 100 mm. EDX results of gray area inside

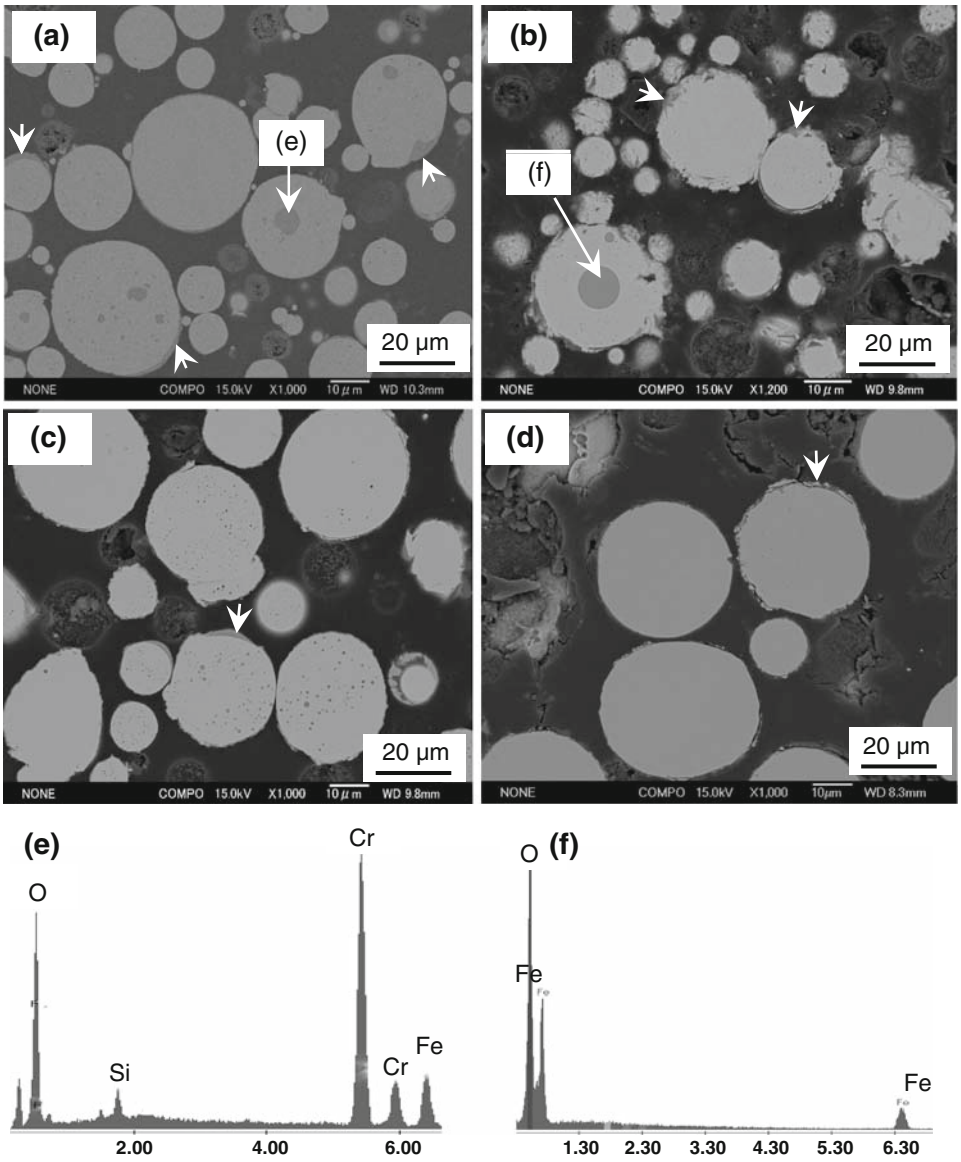

Fig. 2 Cross-sectional BSE images and EDX results on gray areas of captured particles at SD 100 mm. (a) SUS316L; (b) Pure iron; (c) Fe1Si; (d) Fe1B, and EDX result of gray phase: (e) marked in (a), (f) marked in (b)

iron and SUS316L particles are shown in Fig. 2(e) and (f), respectively. Gray contrast nodules were apparent inside the AISI 316L and iron particles (Fig. 2a and b). Very small gray nodules were also present in the Fe1Si particles (Fig. 2c), while the Fe1B particles had a uniform microstructure (Fig. 2d). The gray contrast layers on the surfaces were observed in all the particles as indicated by white arrows. The results from the EDX analysis revealed that the gray phases were Fe oxides as same as that shown in Fig. 2(f) for Fe-Si and Fe-B particles. For AISI 316L particles, the gray phases were Fe oxides containing Cr and Si (Fig. 2e).

Figure 3 shows elemental map image of the cross section of Fe1B particles captured at SD 200 mm. Comparing with the particles captured at SD 100 mm (Fig. 2d), Fe oxides layers and nodules are revealed apparently on the surface and inside the particles captured at SD 200 mm, respectively. From the B and O map images of Fig. 3(c) and (d), particles with higher B concentration (indicated by white arrows) contained no oxides in them. The result indicates that the oxide content increased with an increase in SD from 100 to 200 mm, and the oxides formed in the particles with lower B contents.

3.1.2 Contents of Oxygen in Sprayed Coatings. The oxygen contents in the coatings of AISI 316L, iron, Fe1Si, and Fe1B are shown in Fig. 4. The oxygen contents in these coatings increased with the increases in SD. Contrary to the well-known effect of Cr in decreasing the oxidation of solid alloys, it did not show such effect during plasma spraying, i.e., the oxidation of SUS316L and the pure iron coatings were not different. Addition of

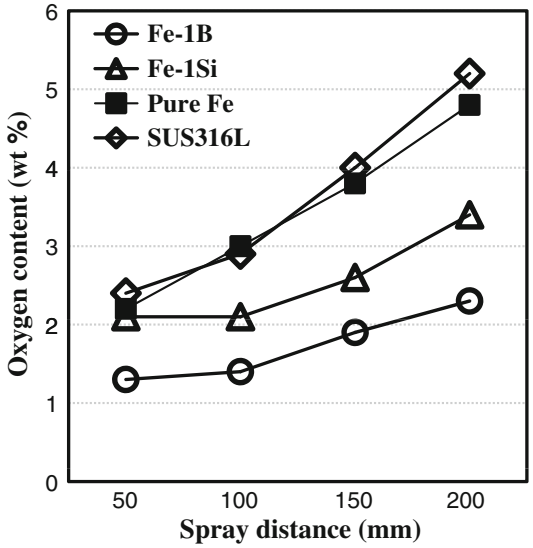

Fig. 4 Oxygen contents in the coatings of SUS316, iron, Fe1Si, and Fe1B with increases in SD

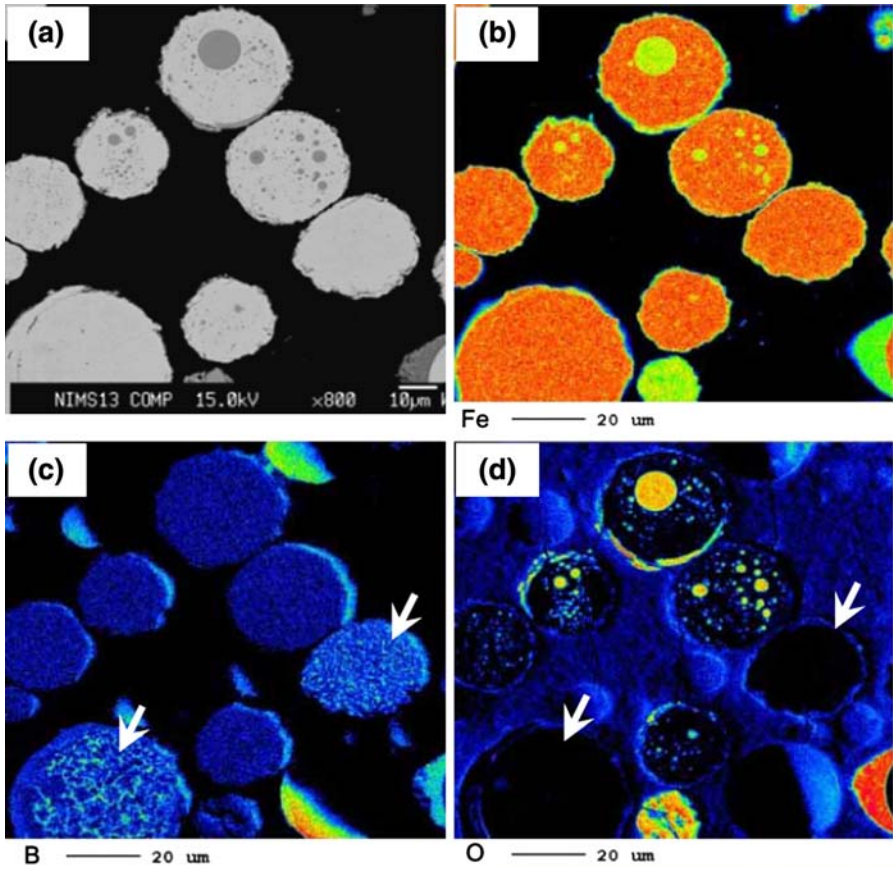

Fig. 3 BSE image and elemental mappings of the cross section of Fe1B particles captured at SD 200 mm

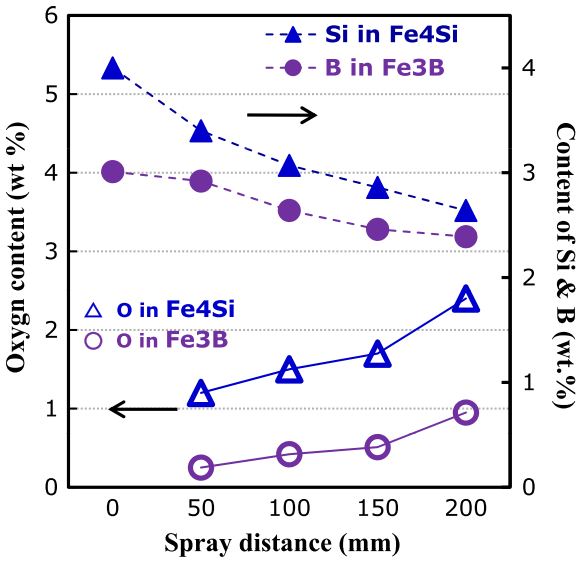

Fig. 5 Contents of oxygen, silicon, and boron in coatings of Fe-4Si and Fe-3B with increases in SD

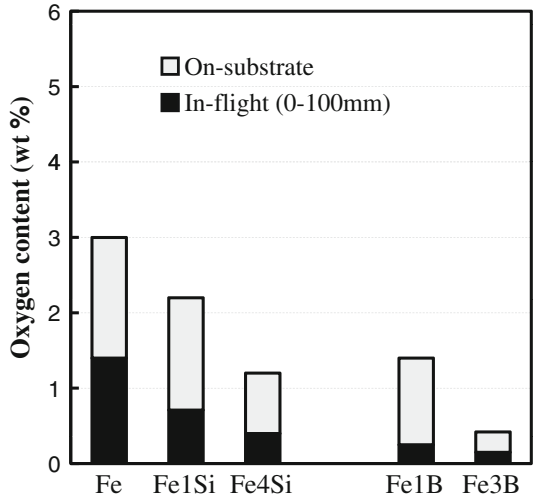

Fig. 6 Oxygen gained during in-flight and after impacting substrate for Fe-alloy coatings sprayed at SD 100 mm

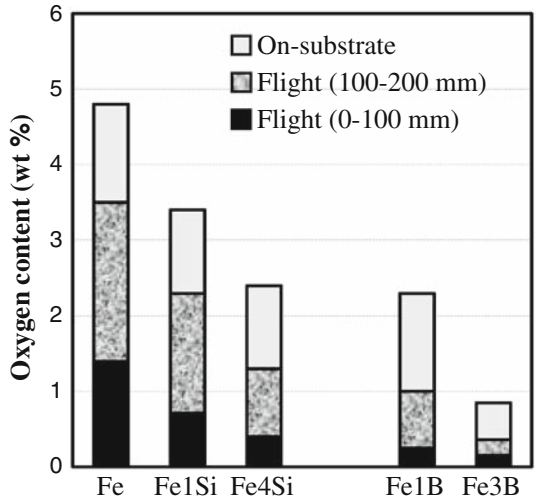

Fig. 7 Oxygen gained during in-flight and after impacting substrate for Fe-alloy coatings sprayed at SD 200 mm

silicon and boron to iron, however, reduced oxidation significantly.

Figure 5 shows the contents of oxygen, silicon, and boron in the Fe4Si and Fe3B coatings. It is clear that the oxygen contents increased with increases in SD and at same time the contents of Si and B decreased. Comparing with the results of Fe1Si and Fe1B shown in Fig. 4, oxygen contents further reduced by increasing Si and B content from 1 to 4 wt.% and 1 to 3 wt.%, respectively; especially boron affected the most.

3.1.3 In-Flight and On-Substrate Oxidation. The difference in oxygen contents between the captured particles (in-flight oxidation) and the coatings is considered to be the oxygen gain after particle impacting the substrate (on-substrate oxidation). The oxygen contents in the coatings divided into the amount gained during flight and after impacting substrate for the coatings sprayed at SD 100 and 200 mm are shown in Fig. 6 and 7 respectively. From Fig. 6, the oxygen gained during particle flight at SD 100 mm (presented by black bars) decreased for all the Si- and B-added alloys compared with that of iron. The reduction rate of the in-flight oxidation for the Fe1Si and Fe1B coatings to the in-flight oxidation of iron was about 50% and 82%, respectively. Further increasing Si and B contents to 4 wt.% and 3 wt.%, the reduction rate increased to 70% and 90%, respectively.

From Fig. 7 showing the oxygen gained in the coating sprayed at SD 200 mm, the oxygen gained for iron particles during flight from 100 to 200 mm (gray bars) was higher than that during flight from nozzle exit (0 mm) to 100 mm (black bars). It is caused by more air entrance in plasma plume at the longer SD and possibly the longer flight time because the particle velocity may decrease. The reduction rate of in-flight oxidation from SD 100 to 200 mm for the Fe1Si and Fe1B coatings was about 24% and 64%, respectively. Further increasing Si and B contents in iron to respective 4 wt.% and 3 wt.%, the reduction rates of in-flight oxidation increased to 57% and 90%, respectively. The reduction rates were lower than that during flight from the nozzle exit (0 mm) to 100 mm (black bars) for the Fe1Si, Fe4Si, and Fe1B coatings, however, for Fe3B, the reduction rate was at the same level.

On-substrate oxidations of the Fe1Si and Fe1B coatings (shown by white bars in Fig. 6 and 7) did not reveal significant differences compared with iron coating, whereas on-substrate oxidation decreased for the Fe4Si and Fe3B coatings. The addition of Si and B to iron reduced the in-flight oxidation significantly. With increases in Si and B content, the reduction of on-substrate oxidation became obvious, especially the B affected the most.

Figure 8 shows the Si and B contents in the feedstock powders, captured particles and sprayed coatings of Fe1Si, Fe4Si, Fe1B, and F3B alloys at SD 100 mm. It is clear that all the Si and B content decreased in the captured particles and coatings as compared to the respective feedstock powders. It is noticed that the content of Si and B in the captured particles and in the respective coating showed no difference. This means the loss of Si and B occurred during particle flight instead of after particle impact.

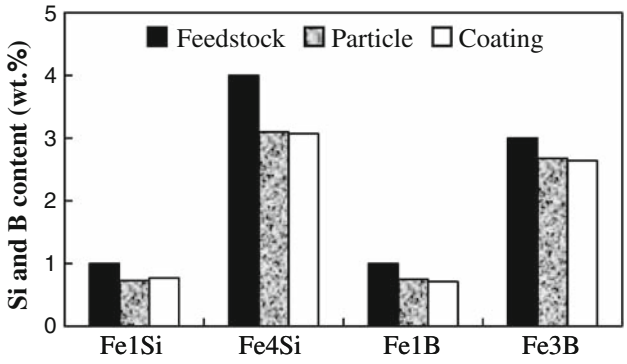

Fig. 8 Silicon and boron contents in the feedstock powders, captured particles and coatings at SD 100 mm of Fe-Si and Fe-B alloys

3.2 Ni-Based Alloys

3.2.1 Cross Section of Captured Particles and Coatings. Figure 9 shows BSE images of the cross sections of captured Ni20Cr and NiCrSiBC particles at SD 100 mm. It is observed from Fig. 9(a) that the gray contrast layer covered the captured Ni20Cr particle and gray contrast nodules were present in the interior. The result of EDX analysis showed that the gray contrast areas are Cr oxides. The cross section microstructures of the captured NiCrSiBC particles (Fig. 9b) presented uniform bright contrast. Some small gray spots were observed in the matrix of the particles (indicated by the arrow). EDX result showed that the gray spots are high in Cr content. Since no significant concentration of oxygen was detected, they are considered to be Cr carbides and borides (Ref 12) as will be revealed by XRD.

Figure 10 shows the cross-sectional microstructures of the Ni20Cr and NiCrSiBC coatings sprayed at SD 100 mm. The primary morphological difference between the two coatings was the presence of a significant quantity of oxides that located mostly at the boundaries of the particles in the Ni20Cr coating (Fig. 10a). For the

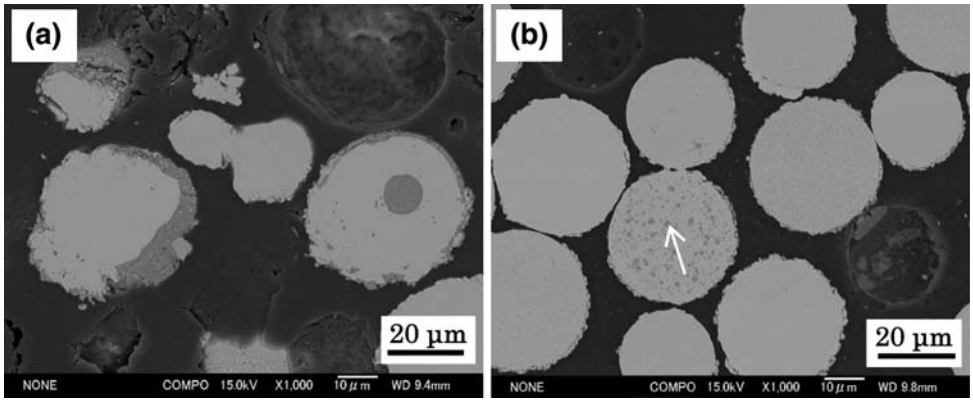

Fig. 9 Cross-sectional BSE images of (a) captured Ni20Cr and (b) NiCrSiBC particles captured at SD 100 mm

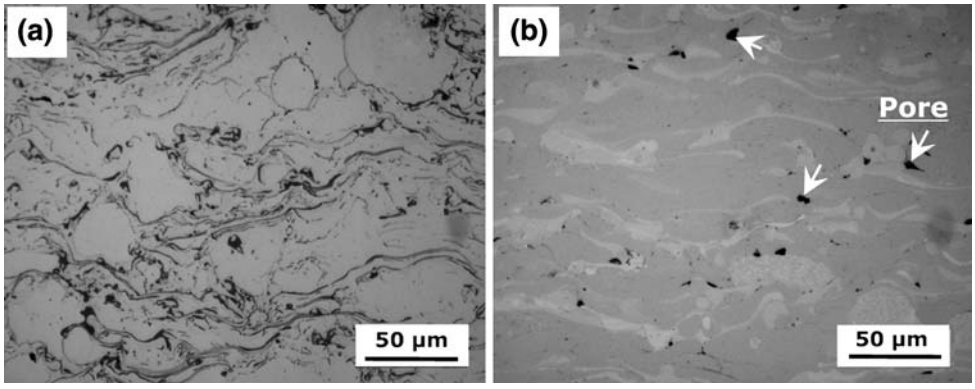

Fig. 10 Cross-sectional microstructures of (a) Ni20Cr and (b) NiCrSiBC coatings sprayed at SD of 100 mm

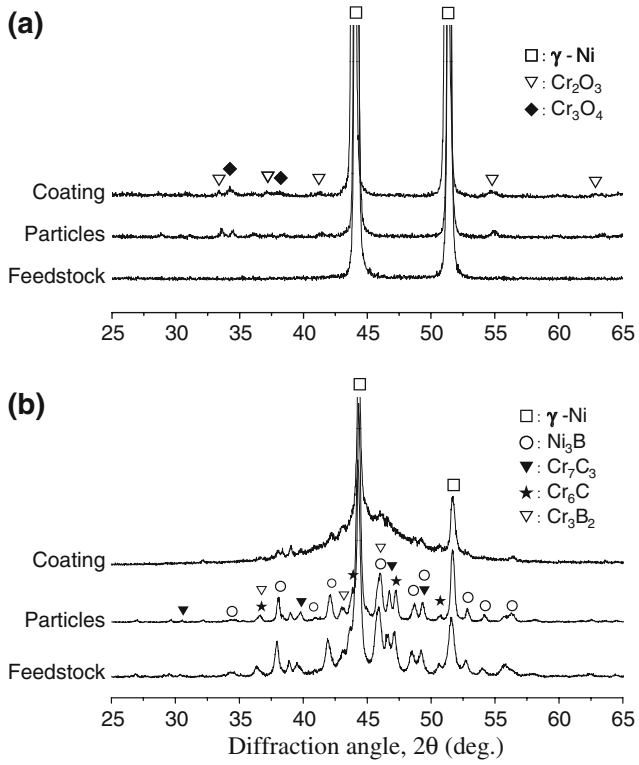

Fig. 11 X-ray diffraction spectra from feedstock, captured particles, and coating. Ni20Cr alloy (a) and NiCrSiBC alloy (b)

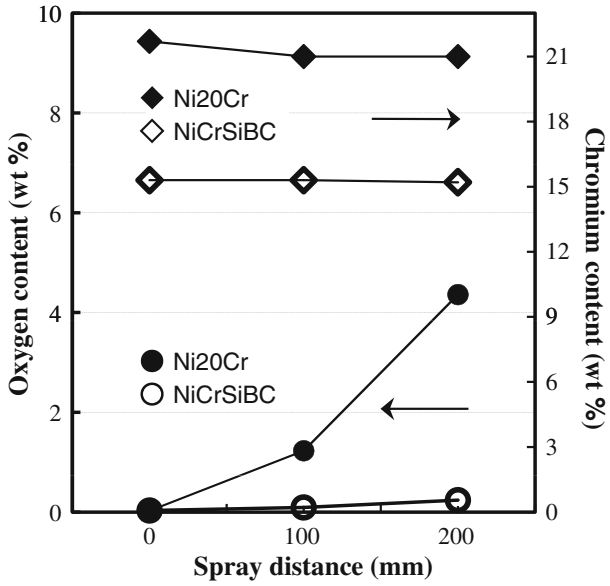

Fig. 12 Contents of oxygen and chromium in the Ni20Cr and NiCrSiBC coatings sprayed at SD 100 and 200 mm

NiCrSiBC coating (Fig. 10b), oxides were not detected by EDX analysis. The black spots in the NiCrSiBC coating were found to be porosity rather than oxides (indicated by the arrows).

Another difference was that the Ni20Cr coating contained unmelted round particles; in contrast, most of the particles were well flattened in the NiCrSiBC coating. This indicates that the plasma powder by the spray parameter was not enough to melt all Ni20Cr particles because the higher melting point of 1400 °C for the Ni20Cr feedstock comparing with a melting point of 1050 °C for the NiCrSiB powder.

XRD diffraction results of the feedstock powder, the captured particles and the coating at SD 100 mm are shown in Fig. 11. For Ni20Cr alloy shown in Fig. 11(a), in addition to the single γ phase of the feedstock material, some Cr_2O_3 and Cr_3O_4 peaks are found in the captured particles and the coating. For the NiCrSiBC alloy shown in Fig. 11(b), many peaks observed are indexed as the compounds such as Ni_3B, Cr_7C_3, Cr_6C, and Cr_3B_2, and no oxide peak is detected. Comparing the spectrum of the coating with that of the feedstock powder and the captured particles, a very broad peak at 2θ of 40°-50° is observed from the coating. This indicates that the coating matrix consists of an amorphous phase or very fine grains, which implies that the cooling rate on the substrate was the highest (10^7-10^8 K s^{-1}) (Ref 13) as compared to the cooling rates experienced during the gas atomization for the feedstock production or the cooling in liquid nitrogen for the capturing of particles (10^5-10^6 K s^{-1}) (Ref 14, 15).

3.2.2 Changes of Elemental Content in the Captured Particles. Figure 12 shows the contents of oxygen and chromium in the Ni20Cr and NiCrSiBC coatings sprayed at SD 100 and 200 mm. The oxygen contents in the Ni20Cr coatings were significantly higher than that in the NiCrSiBC coatings by a factor of 13 and 20 for the coatings sprayed at 100 and 200 mm, respectively. The oxygen content of the NiCiSiBC coatings showed almost no changes when sprayed at SD 100 mm, and very limited increases in the coating sprayed at 200 mm. The chromium content decreased for the Ni20Cr coating sprayed at 100 mm as compared with the content in the feedstock. In contrast, the chromium content did not show any obvious change in the NiCrSiBC coatings sprayed at SD 100 and 200 mm.

Figure 13 shows the changes in the content of C, Si, and B in the NiCrSiBC coatings with increases in SD. It shows a tendency of decrease in the contents of C, Si, and B in the coatings compared with that in the feedstock. The decreases in Si and B increased with increases in SD; however, C decrease occurred within SD 100 mm, and it showed no further decrease when SD became longer than 100 mm. By comparing with the oxygen contents in Fig. 12, the zero oxygen gained in the coating sprayed at SD 100 mm must be related to the loss of these elements during the spraying process.

3.3 Discussion

The results presented in this study demonstrate that the addition of Si, B to iron and Si, B, and C to Ni-Cr alloy decreased the oxidation of these alloys during APS significantly.

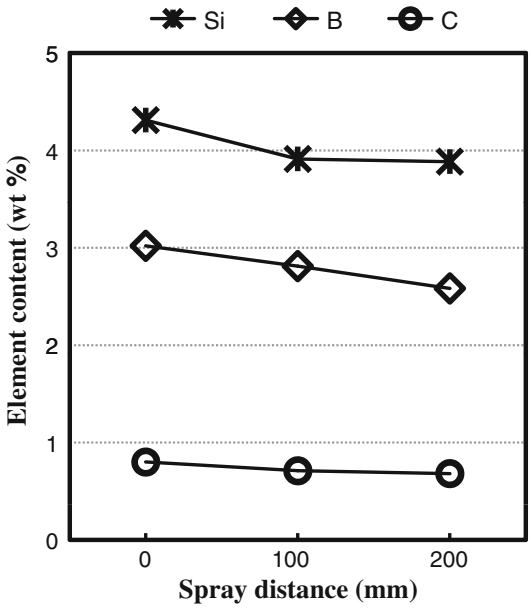

Fig. 13 Contents of C, Si, and B with increases in SD in the NiCrSiBC coatings

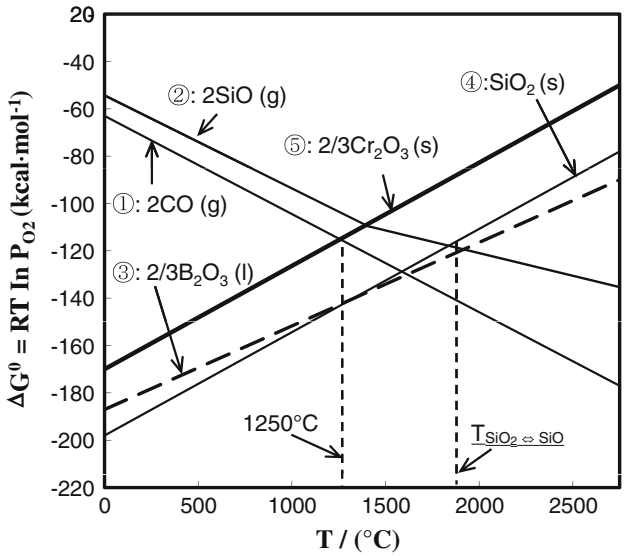

Fig. 14 A diagram of standard free energy of oxide formation for the element

Figure 14 shows a diagram of standard free energy of oxide formation for the elements of C, B, Si, and Cr drawn by using data from handbook (Ref 16, 17). Since Ni and Fe are more stable than Cr, only Cr is plotted here. Based on the diagram, the oxidation reactions to form CO, SiO, and B_2O_3 should occur preferentially than forming Cr_2O_3 at higher temperature over 1250 °C. In the APS process, the high process temperature, which is much higher than the melting point of the alloy particles containing Si, B, and C, possibly causes the formation of gaseous oxides of SiO, CO, and evaporable B_2O_3. These reactions lead to the decrease in the contents of C, Si, and B in the alloy, resulting in suppressions of Fe and Cr oxidation.

The oxygen content of the in-flight particles of Fe-binary alloys decreased significantly, and at the same time the loss of Si, B occurred (Fig. 6 and 8). The higher temperature favored the formation of evaporable SiO and B_2O_3 oxides than FeO. This study showed B was the most effective for reduction of oxidation of iron.

The remarkably low oxidation in the NiCrSiBC coating is believed to be a combined effects of the alloying elements of C, Si, and B. Carbon directly forms gaseous oxides whereas the formed oxides of Si and B evaporate, lowering the oxygen content around the surface of the molten particles and suppressing the oxide formation on the surface of the droplets.

Since there are no such elements to act as oxygen absorbers in the molten Ni20Cr and SUS316L particles, significant Cr oxidation took place, to form Cr containing oxides in the particles and coatings (Fig. 2 and 11).

4. Summary

Fe-binary alloy powders with addition of Si (1 and 4 wt.%) or B (1 and 3 wt.%) and a Ni-Cr based alloy powder with Si (4.3 wt.%), B (3.0 wt.%), and C (0.8 wt.%) additions were sprayed by atmospheric plasma spray. The benefit from additions of Si, B, and C to iron and Ni-Cr alloy to reduce the oxide content of the coatings was quantified.

Addition of 1 wt.% Si and 1 wt.% B to pure Fe reduced oxygen contents in the coatings by 50% and 82%, respectively, at SD of 100 mm. With increases in the contents of Si and B from 1 to 4 and 3 wt.%, respectively, the reduction ratio in the coatings increased further to 70% and 90%, respectively. Addition of these elements was more effective for reducing the in-flight oxidation as compared to the on-substrate oxidation.

The oxygen content in Ni20Cr coating was significantly higher than that of NiCrSiBC coating by a factor of 13 for the coating sprayed at 100 mm. Almost no oxygen pickup occurred in the NiCrSiBC coatings because of the preferential oxidation of C, Si, and B and the formation of their gaseous oxides.

Sacrificial oxidation of Si, B, and C was shown to be highly effective to control the oxidation of plasma-sprayed iron and Ni-Cr based alloys.

References

1. D. Shin, F. Gitzhofer, and C. Moreau, Properties of Induction Plasma Sprayed Iron Based Nanostructure Alloy Coatings for Metal Based Thermal Barrier Coatings, *J. Therm. Spray Technol.*, 2007, **16**(1), p 118-127
2. K. Kishitake, H. Era, and F. Otsubo, Thermal-Sprayed Fe-10Cr-13P-7C Amorphous Coatings Possessing Excellent Corrosion Resistance, *J. Therm. Spray Technol.*, 1996, **5**(4), p 476-482
3. T. Sundararajan, S. Kuraoda, K. Nishida, T. Itagaki, and F. Abe, Behaviour of Mn and Si in the Spray Powders during Steam

Oxidation of Ni-Cr Thermal Spray Coatings, *ISIJ Int.*, 2004, **1**, p 139-144
4. S. Kuroda and S. Kitahara, Current Status and Future Trends, *Proc. Therm. Spraying*, A. Ohmori, Ed., May 22-26 (Kobe, Japan), High Temperature Society of Japan, 1995, p 489-494
5. B.S. Sidhu and S. Prakash, Nickel-Chromium Plasma Spray Coatings: A Way to Enhance Degradation Resistance of Boiler Tube Steels in *Boiler Environment*, *J. Thermal Spray Technol.*, 2006, **15**(1), p 131-140
6. T.S. Sidhu, S. Prakash, and R.D. Agrawa, Characterization of HVOF Sprayed NiCrSiBSi Coatings on Ni- and Fe-based Superalloys in Molten Salt Environment, *Thin Solid Films*, 2006, **515**, p 95-105
7. A.A. Syed, A. Denoirjean, P. Fauchais, and J.C. Labbe, On the Oxidation of Stainless Steel Particles in the Plasma Jet, *Surf. Coat. Technol.*, 2006, **200**, p 4368-4382
8. Z. Zeng, N. Sakoda, T. Tajiri, and S. Kuroda, Structure and Corrosion Behavior of 316L Stainless Steel Coatings Formed by HVAF Spraying With and Without Sealing, *Surf. Coat Technol.*, 2008, **203**, p 284-290
9. S.H. Zahiri, D. Fraser, S. Gullizia, and M. Jahedi, Effect of Processing Conditions on Porosity Formation in Cold Gas Dynamic Spraying of Copper, *J. Thermal Spray Technol.*, 2006, **15**(3), p 422-430
10. H. Sun and R.D. Pehlke, Modeling and Experimental Study of Gaseous Oxidation of Liquid Iron Alloys, *Metall. Mater. Trans. B*, 1996, **27**, p 854-864
11. Y. Kawai and K. Mori, Rate of Oxidation of Silicon in Liquid Iron by Oxidation Gas, *Iron Steel*, 1970, **56**(6), p 35-47
12. K. Kishitake, H. Era, and F. Otsubo, Structure and Phases in Nickel-Based Self Fluxing Alloy Coating, *J. Jpn Weld. Soc.*, 2000, **18**(1), p 126-132
13. S. Sampath and H. Herman, Rapid Solidification and Microstructure Development during Plasma Spray Deposition, *J. Thermal Spray Technol.*, 1996, **5**, p 445-456
14. M.R. Libera, P.P. Bolsaits, R. Erik Spjut, and J.B. Vander Sande, Liquid Supercooling and Droplet cooling rates of Remelted Argon Atomized Fe-30Ni powder Particles, *J. Mater. Res.*, 1988, **3**, p 441
15. P. Kotalik and K. Volenik, *J. Phys. D Appl. Phys.*, 2001, **34**, p 567
16. *Hand Book of Iron and Steel*, 3rd edn. The Japan Institute of Metals, Maruzen Company, Japan, 1971, p 241-326
17. Z.D. Yang, S.L. Liu, X.X. Xue, H.M. Chang, L. Oing, and H.L. Ma, Oxidation of Carbon in Iron Melt Containing Boron and Silicon, *J. Iron Steel Res.*, 2006, **18**, p 6 (in Chinese)